Differential response at the seafloor during Paleocene and Eocene ocean warming events at Walvis Ridge, Atlantic Ocean (ODP Site 1262)

Arne Deprez[1]*, Sofie Jehle[2], André Bornemann[2,3] and Robert P. Speijer[1]

[1]*Department of Earth and Environmental Sciences, KU Leuven, 3001 Heverlee, Belgium*

[2]*Institut für Geophysik und Geologie, Universität Leipzig, 04103 Leipzig, Germany*

[3]*Bundesanstalt für Geowissenschaften und Rohstoffe, 30655 Hannover, Germany*

** corresponding author:+32 16 37 21 95, arne.deprez@kuleuven.be*

This is the accepted version of the following article:

Deprez, A., Jehle, S., Bornemann, A., Speijer, R.P., 2017. Differential response at the seafloor during Palaeocene and Eocene ocean warming events at Walvis Ridge, Atlantic Ocean (ODP Site 1262). Terra Nova 29 (1), 71-76.

which has been published in final form at http://dx.doi.org/10.1111/ter.12250. This version lacks final copy-editing, but no changes to the scientific content were made.

Abstract

The Latest Danian Event (LDE, ~62.1 Ma) is an early Paleogene hyperthermal or transient (<200 kyr) ocean warming event. We present the first deep-sea benthic foraminiferal faunal record to study deep-sea biotic changes and new benthic (*Nuttallides truempyi*) stable isotope data from Walvis Ridge Site 1262 (Atlantic Ocean) to evaluate whether the LDE is controlled by similar processes as the minor early Eocene hyperthermals. The spacing of the double negative $\delta^{13}C$ and $\delta^{18}O$ excursion and the slope of the $\delta^{18}O$-$\delta^{13}C$ regression is comparable, strongly suggesting a similar orbital control and pacing of eccentricity maxima as well as a rather homogeneous carbon pool. However, in contrast to early Eocene hyperthermals, the benthic foraminiferal fauna is remarkably stable across the LDE. This lack of benthic response could be related to the absence of threshold related circulation changes or better pre-adaptation to elevated deep-sea temperatures, as the LDE was superimposed on a cooling trend, in contrast to early Eocene warming.

Introduction

The early Paleogene is characterized by numerous hyperthermals, transient (<200 kyr) deep-sea and surface ocean warming events, associated with carbon isotope excursions (CIEs) and carbonate dissolution in the deep sea. Of these, the Paleocene-Eocene Thermal Maximum (PETM; ~56 Ma) is the most extreme example. The Latest Danian Event (LDE; Bornemann *et al.*, 2009; ~62.1 Ma), also referred to as Top Chron 27n Event (Westerhold *et al.*, 2011) is a minor hyperthermal compared to the PETM. Benthic and planktic foraminiferal isotope records indicate a ~2-3°C warming (Westerhold *et al.*, 2011; Jehle *et al.*, 2015), and a ~0.7‰ negative CIE (Bornemann *et al.*, 2009; Westerhold *et al.*, 2011). Also peak values in XRF core scanning Fe records (Westerhold *et al.*, 2008), anoxia in marginal basins (Sprong *et al.*, 2012, Schulte *et al.*, 2013) and biotic changes among calcareous nannofossils (Monechi *et al.*, 2013), planktic foraminifera (Jehle *et al.*, 2015) and mammals (Clyde *et al.*, 2008) coinciding with the LDE are strongly reminiscent phenomena related to the PETM. At present, it is

unclear whether the LDE was controlled by similar processes as the minor early Eocene hyperthermals. Also the biotic changes in the deep-sea have not been studied so far.

This paper provides the first in-depth comparison between isotope records spanning the LDE and the Eocene ETM2-H2 hyperthermals, as recorded at Walvis Ridge ODP Site 1262 (Stap *et al.*, 2010). We combine the isotopic data with benthic foraminiferal abundance patterns in order to evaluate relationships between transient warming events and development of the early Paleogene deep sea ecosystem.

Walvis Ridge ODP Site 1262 is located at 4759 m water depth near the base of Walvis Ridge (Angola Basin). Paleocene sediments consist of nannofossil ooze with cyclic variations in sediment lightness and geochemistry, representing a response to orbital forcing (Westerhold *et al.*, 2008). Paleodepth was estimated as ~3000 – 3300 m, based on a simple thermal subsidence model and benthic foraminiferal assemblages (Shipboard Scientific Party, 2004a; b).

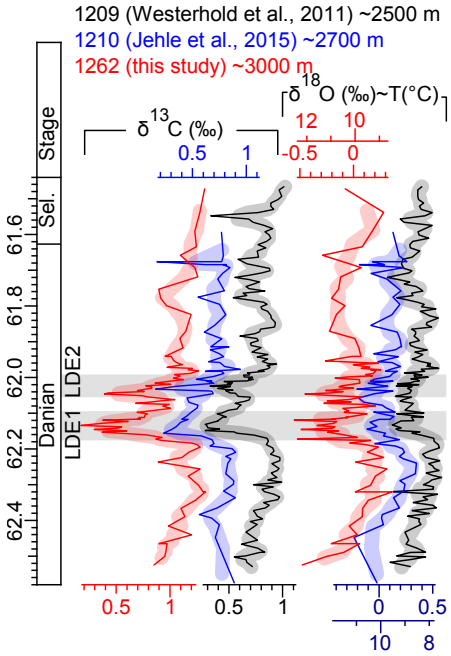

Fig. 1. Nuttallides truempyi isotope patterns of ODP Sites 1209, 1210 (Shatsky Rise, Pacific Ocean) and 1262 (Walvis Ridge, Atlantic Ocean) plotted against the numeric age model based on linear interpolation between short-term eccentricity maxima of Westerhold et al. (2008), option 2. Thick lines represent a 3-point moving average. Records from Walvis Ridge and $\delta^{13}C$ records were plotted on a different scale to prevent overlapping records. Temperature estimates are according to the Erez and Luz (1983) paleotemperature calculation with 1.2‰ ice-free standard mean ocean water (Shackleton and Kennett, 1975) and a 0.35‰ correction for Nuttallides vital effects (Shackleton et al., 1984).

Material and methods

Stable isotopes ratios ($\delta^{18}O$, $\delta^{13}C$) for 91 samples from 9 m of core were measured on five *Nuttallides truempyi* specimens (size 125-180 µm) per sample (Appendix S1). SEM images of broken *N. truempyi* (Appendix S2) reveal open pores, but also the presence of ~1 µm sized crystals of secondary calcite on interior walls. Since most recrystallization takes place in the upper sediment layers, benthic foraminifera preserve the stable isotope signature, even if recrystallized (Edgar *et al.*, 2013; Voigt *et al.*, 2016). Regression lines were calculated to investigate the relationship between the $\delta^{13}C$ and the $\delta^{18}O$ excursion. Major axis regression was used instead of ordinary least squares, because of measurement errors associated with both $\delta^{13}C$ and $\delta^{18}O$. Slopes were compared to major axis regression for early Eocene hyperthermals (data from Lauretano *et al.*, 2015). Sedimentary $CaCO_3$ was determined using a LECO device at the BGR in Hannover.

Benthic foraminiferal abundances were obtained from representative splits (> 270 specimens) of the >63 µm fraction. Benthic foraminifera were classified in epibenthic and endobenthic morphotypes according to Corliss and Chen (1988). Shannon diversity was calculated based on the dataset with absolute counts (Hammer, 2015). Benthic foraminiferal accumulation rates (BFAR) were calculated by multiplication of foraminiferal numbers per gram with sedimentation rates (option 2 age model of Westerhold *et al.*, 2008) and Shipboard dry bulk densities (Shipboard Scientific Party, 2004b). Non-metric multidimensional scaling (NMDS) on abundances for all taxa with a maximum relative abundance >2% was run to identify the main patterns in the benthic foraminiferal abundances. The

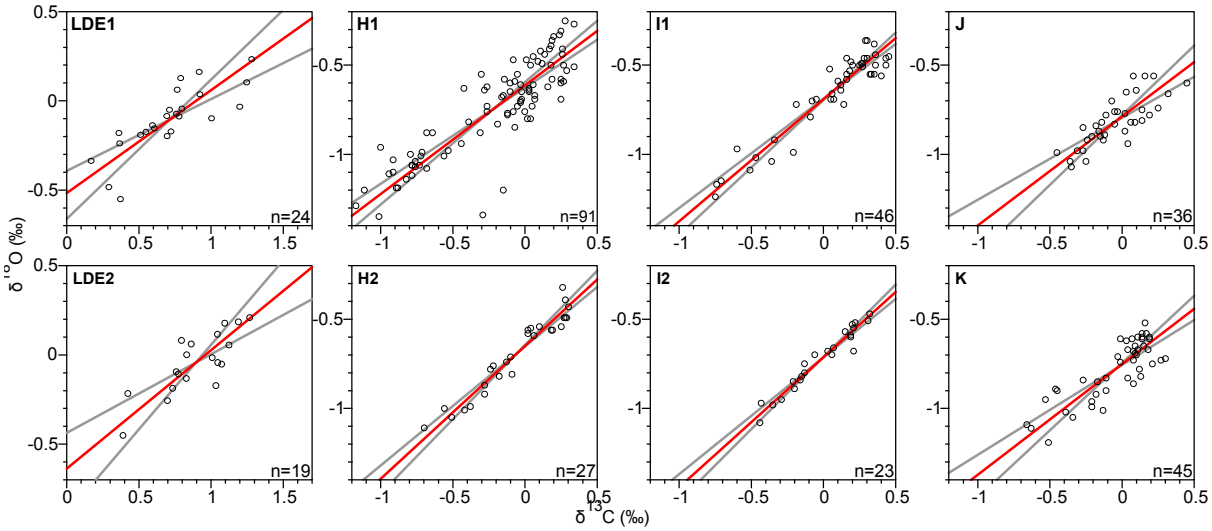

Fig. 2. Cross-plots for $\delta^{13}C$ and $\delta^{18}O$ for LDE1, LDE2, H1 (ETM2), H2, I1, I2, J and K (ETM3). All graphs show the regression line (major regression) in red and confidence intervals in gray. The major regression line shows similar relationships for $\delta^{13}C$ and $\delta^{18}O$ throughout the event for LDE1, H1, I1, J and K. Also LDE2, H2 and I2 have similar $\delta^{13}C$-$\delta^{18}O$ slopes. Data for Eocene events from Lauretano et al. (2015). The number of observations for each event is indicated in the lower right corner.

2D representation and the correlation distance measure were chosen (e.g. Hammer and Harper, 2006). To compare the LDE to early Eocene hyperthermals, Σ_{CV} were calculated following the biotic scaling approach of Gibbs *et al.* (2012). This measure associates one value to the overall assemblage variability in a certain time period. These were calculated on a dataset with 3 point moving averages of all taxa with an average abundance of more than 1%. More information on material and methods is available in Appendix S3.

Results and discussion

Stable isotopes

The isotopic record (Fig. 1) reveals two distinct negative peaks, both in $\delta^{13}C$ and $\delta^{18}O$ at ~62.1 Ma (~195 mcd), here termed LDE1 and LDE2. These two peaks coincide with higher Fe, as revealed by XRF core scanning (Westerhold *et al.*, 2008) and lower carbonate values (Fig. 4). LDE1 at Walvis Ridge starts at 62.18 Ma (195.6 mcd), reaching lowest $\delta^{13}C$ values at 62.14 Ma (195.3 mcd). This CIE coincides with a ~0.5‰ negative $\delta^{18}O$ excursion, indicating ~2.2°C bottom water warming, assuming no local changes in $\delta^{18}O_{SW}$ due to salinity or ice volume. LDE2 peaks at 62.04 Ma (194.5 mcd) with a ~0.5‰ CIE and a ~0.3‰ $\delta^{18}O$ excursion. Both isotopic records return to pre-LDE values in about 50 kyr at 61.99 Ma (194.1 mcd).

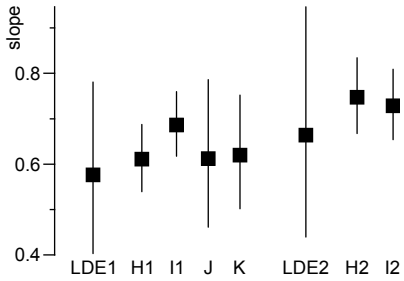

Fig. 3. Calculated slopes and 95% confidence intervals of major axis regression of all studied hyperthermals. Number of observations for each event are indicated in Fig. 2. Second events of a hyperthermal pair are indicated on the right.

These peaks correspond to those observed at Shatsky Rise sites 1209 and 1210, but Site 1262 shows a larger CIE (0.9 compared to 0.6‰) and warming (2.2 compared to 1.5-2°C) during LDE1. The LDE shows a pattern of two CIEs, 100 kyr apart, which it shares with ETM2-H2, and I1-I2 (Littler *et al.*, 2014). All these CIEs are thought to relate to short-term (100 kyr) eccentricity maxima in one long-term (400 kyr) eccentricity maximum (Westerhold *et al.*, 2008;

Hilgen *et al.*, 2015). The slopes of major axis regression (Fig. 2) on the $\delta^{13}C$-$\delta^{18}O$ relationship for the LDE and early Eocene hyperthermals are plotted in Fig. 3. Compared to slopes for early Eocene hyperthermals, LDE1 has a similar slope to H1 (ETM2), J and K (ETM3). I1 has a slightly steeper slope than the other events, but still within the 95% confidence intervals of all other events. LDE2 has a steeper slope then LDE1, but compared to the other secondary events in a hyperthermal pair, H2 and I2, it is in the lower range of the confidence interval. The relationship between the added mass of carbon divided by the initial mass of carbon in the ocean-atmosphere system ($M_{added}/M_{initial}$) and the $\delta^{13}C$ change is given by $M_{added} / M_{initial} = -CIE / (\delta^{13}C_{final} - \delta^{13}C_{added})$ (McInerney and Wing, 2011). The slope of the relationship between $\delta^{13}C$ and $\delta^{18}O$ is dependent on climate sensitivity (temperature change per increase in CO_2) and the $\delta^{13}C$ value of the source of reduced carbon. Climate sensitivity governs the relationship between $\delta^{18}O$ (as measure for temperature) and the amount of carbon added to the atmosphere ($M_{added} / M_{initial}$). For more negative values for the carbon source, $\delta^{13}C_{final} - \delta^{13}C_{added}$ increases and the slope ($1 / (\delta^{13}C_{final} - \delta^{13}C_{added})$) is less steep. Similar slopes thus point to similar climate sensitivities for Paleocene and Eocene hyperthermals and a similar carbon source, although compensating effects of both factors are also possible.

The difference in slope between the primary and secondary events was noted by Lauretano *et al.* (2015). Possible causes for this difference include a higher contribution of an isotopically less negative source during the secondary events (because of incomplete filling of the carbon reservoir; Dickens, 2003), different climate feedbacks or local changes in circulation. The slope difference between the two LDE peaks could be caused by similar factors.

Four options can account for small changes in the slope of the $\delta^{13}C$-$\delta^{18}O$ regression for hyperthermals. The background $\delta^{13}C$ values of the LDE are more positive because of long-term secular changes. Such higher background values will cause a lower slope for the LDE, because the difference with the isotope signature of the source is larger. Then, the $\delta^{13}C$ of the ocean-atmosphere system changes more rapidly for an equal CO_2 rise. Alternatively, this slight change can reflect changes in climate sensitivity, as climate sensitivity seems to be higher at higher temperatures (Caballero and Huber, 2013; von der Heydt *et al.*, 2014). The LDE is superimposed on a cooler climate than Eocene hyperthermals, and has a shallower slope (less $\delta^{18}O$ change per unit change in $\delta^{13}C$), as expected. A third option for differences in slope is a different isotope signature of the source. Relatively small differences in the isotope signature of the source can be caused by changes in atmospheric $\delta^{13}C$, which is certainly the case if a reservoir is emptied during the hyperthermal and gradually filled afterwards (Dickens, 2003). As a last option, changes in climate and atmospheric CO_2 concentration are able to cause changes in carbon fractionation of land plants (Diefendorf *et al.*, 2010; Schubert and Jahren, 2012). The first and the third options can cancel out each other, as continuous fractionation between the atmosphere-ocean system and the carbon source is maintained by continuous refilling of the carbon source from ambient CO_2. In this case, changing climate sensitivity would be responsible for the changing slope.

Similarities in isotopic composition of the carbon source and orbital configuration point to carbon input from a common reduced carbon reservoir causing both the LDE and the double peaked early Eocene hyperthermals. The exact nature of this reduced carbon reservoir is still uncertain, but several release mechanisms have been proposed, such as the destabilization of gas hydrates due to deep-sea circulation changes, peat oxygenation by longer dry seasons or destabilization of permafrost during eccentricity maxima (Lunt *et al.*, 2010; Zachos *et al.*, 2010, DeConto *et al.*, 2012).

Benthic foraminifera

Despite the marked benthic isotopic signature of the LDE and its similarity with the Eocene hyperthermals, especially ETM2-H2, the benthic foraminiferal record for the LDE of Site 1262 (Fig. 4) shows remarkable stability at the seafloor. The first, and most important,

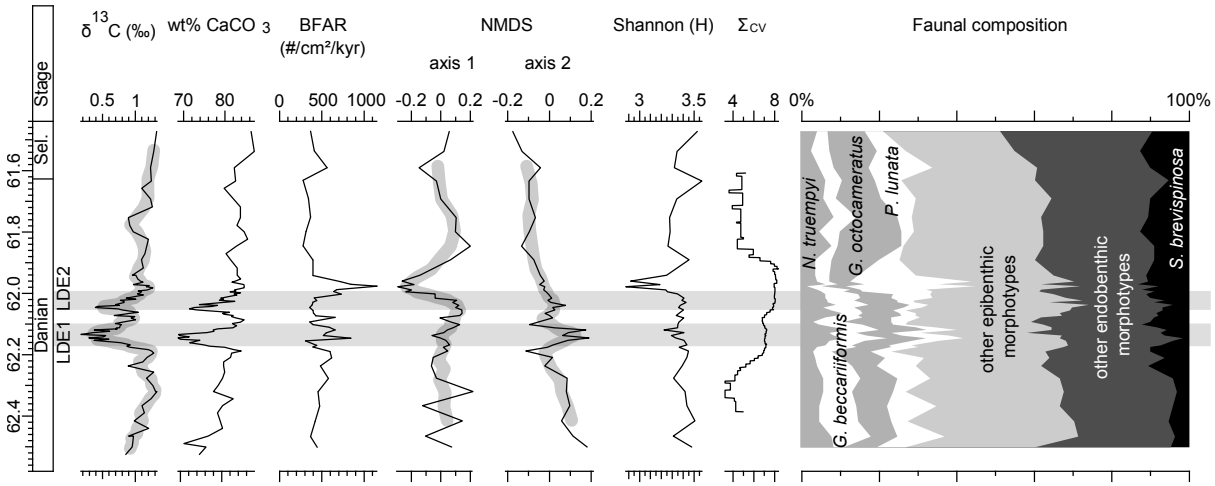

Fig. 4. $\delta^{13}C$ patterns, weight percentage of carbonate on bulk samples, benthic foraminiferal accumulation rates (numbers per cm² per kyr), first and second NMDS axes of benthic foraminiferal relative abundances, Shannon diversity, Σ_{CV} calculated for a sliding time window of 150 kyr, symmetric about the data point and relative abundances of epi- and endobenthic morphotypes and the five most abundant benthic foraminifera: N. truempyi, Gavelinella beccariiformis, Gyroidinoides octocameratus, P. lunata *and* Siphogenerinoides brevispinosa. *All faunal data are reported in Appendix S1*.

NMDS axis shows no faunal change at the base of the LDE It separates a distinct biofacies just above the second LDE peak, coinciding with higher abundances of *Paralabamina lunata*. This species possibly feeds on a specific kind of fresh phytodetritus that is not consumed by other benthic foraminifera. Axis 2, which is less important, shows a small positive excursion in both LDE peaks, coinciding with somewhat higher abundances of *N. truempyi* (from ~5 to ~9%) and other epibenthic morphotypes. Yet, as indicated by the low correlation to initial distances (R^2=0.08), this axis hardly explains the main faunal patterns. On the other hand, a higher abundance of *N. truempyi* and epibenthic morphotypes generally points to more oligotrophic conditions (Thomas, 1998), consistent with lower BFAR (from ~500 to ~400/cm²/kyr) during most of the LDE.

Table 1. Overview of data about hyperthermals. The table includes the slopes (Fig. 3), $\delta^{18}O$ values pre-event, and 300 kyr before the event, peak values and excursion sizes, $\delta^{13}C$ pre-event, peak values and excursion sizes and temperature trends prior to the event, peak values and excursion sizes. Isotope records for Eocene events are from Lauretano et al. (2015).

event	**slope**	**300ka prior to event**	**pre-event**	**trend**	**pre-event**	**peak values**			**excursion**		
		$\delta^{18}O$	**$\delta^{18}O$**	**T(°C)**	**$\delta^{13}C$**	**$\delta^{13}C$**	**$\delta^{18}O$**	**T(°C)**	**$\delta^{13}C$**	**$\delta^{18}O$**	**T(°C)**
LDE1	0.576	-0.1	0.2	-1.3	1.3	0.4	-0.3	11.4	0.9	0.5	2.2
H1 (ETM2)	0.611	-0.3	-0.2	0.2	0.3	-1	-1	14.5	1.3	0.8	3.6
I1	0.686	-0.4	-0.5	0.4	0.4	-0.6	-1.2	15.4	1	0.7	3.1
J	0.612	-0.5	-0.6	0.4	0.3	-0.2	-0.9	14.1	0.5	0.3	1.3
K (ETM3)	0.620	-0.5	-0.6	0.4	0.2	-0.6	-1.1	15.0	0.8	0.5	2.2
LDE2	0.664		0		0.9	0.4	-0.3	11.4	0.5	0.3	1.3
H2	0.748		-0.4		0.2	-0.6	-1	14.5	0.8	0.6	2.7
I2	0.729		-0.5		0.4	-0.3	-1	14.5	0.7	0.5	2.2

An increasing relative abundance of *N. truempyi* and epifaunal morphotypes is also reported at Walvis Ridge during the PETM (Thomas, 2007), ETM2 (Jennions *et al.*, 2015) and ETM3 (Röhl *et al.*, 2006), in addition to higher numbers of abyssaminids during the Eocene events. However, increases in relative abundance of *N. truempyi* and *Abyssamina poagi* (+10%) and decreases in BFAR (from ~200 to ~10/cm²/kyr) and diversity (from ~35 to ~25 species per 100 counts; Jennions *et al.*, 2015) were much larger during ETM2. The increased abundance of thin-shelled *A. poagi* indicates that dissolution is not causing these decreases during ETM2. Comparing Σ_{CV} values, the difference between the events becomes even clearer. The Σ_{CV} of the background Paleocene (pre-LDE) is ~5 (Fig. 4). A Σ_{CV} of ~7 for LDE1 is only slightly larger. Σ_{CV} for ETM2 (data of Jennions *et al.*, 2015) reaches 13. No Eocene background could be assessed, because Jennions *et al.* (2015) only studied the ETM2 event. Overall, the LDE at Walvis Ridge shows comparable faunal changes, but with a much reduced intensity. These minor assemblage changes, however, contrast with CIEs (~0.9‰ for LDE, ~1.4‰ for ETM2, ~0.8‰ for ETM3; Table 1) and temperature change (2°C for LDE1 and ETM3, 4°C for ETM2; Table 1) of nearly identical magnitude.

Short-term deep-sea circulation changes in the Atlantic Ocean were inferred during ETM2 (D'haenens *et al.*, 2014; Jennions *et al.*, 2015) and the PETM (McCarren *et al.*, 2008) in order to explain impoverished benthic foraminiferal assemblages due to oligotrophy (D'haenens *et al.*, 2012) and/or lower dissolved O_2 (McCarren *et al.*, 2008; Jennions *et al.*, 2015). D'haenens *et al.* (2014) suggested that this circulation change was threshold based and these circulation changes were not observed in connection with CIEs slightly smaller than ETM2. The CIE and temperature rise of the LDE is indeed slightly smaller than at ETM2 and ETM3 (Table 1), but absolute bottom water temperatures of ETM2 (~14°C) and ETM3 (~15°C) are significantly higher than these of the LDE (~11°C). The possibility of crossing an absolute temperature threshold is thus higher.

$\delta^{18}O$ data from Shatsky Rise indicate a deep-water long-term cooling trend from 63.0 (~10°C) to 58.5 Ma (~7°C), briefly interrupted during the LDE (Westerhold *et al.*, 2011). The LDE is the only early Paleogene hyperthermal superimposed on such a cooling trend for which the benthic foraminiferal fauna was studied (Table 1). During the LDE, deep-sea temperatures were similar to those prevailing some 0.4 to 1 Ma earlier (Westerhold *et al.*, 2011 and Fig. 1). Under gradually changing conditions, benthic foraminiferal genetic evolution will lag behind environmental change (Lynch and Lande, 1993) because benthic foraminifera evolve slowly (Pawlowski *et al.*, 2007), but can adapt by phenotypic plasticity (Chevin *et al.*, 2010). In a gradually cooling deep-sea, this lag in genetic adaptation would lead to species well-adapted to higher temperatures than the prevailing conditions. Accordingly, a brief interruption of long-term cooling during the LDE would not affect deep-sea communities, as shown by our data.

Conclusions

The early Paleocene LDE hyperthermal event bears some striking similarities in environmental and biotic characterization with the PETM. Furthermore, both the LDE and early Eocene hyperthermals ETM2-H2 and I1-I2 of Site 1262, Walvis Ridge, show orbitally-paced double-peaked $\delta^{13}C$ and $\delta^{18}O$ excursions with a similar relationship between $\delta^{13}C$ and $\delta^{18}O$ changes, strongly suggesting a shared astronomically controlled causal mechanism. Yet, in contrast to ETM2-H2 (and the PETM), benthic foraminiferal faunal patterns show remarkable stability at the seafloor during the LDE. This discrepancy may be explained by the rather cool early Paleocene background deep-sea temperature and the lack of threshold related circulation changes as during the early Eocene hyperthermals. In addition, benthic communities were well-adapted to higher temperatures as the LDE was superimposed on an early Paleocene cooling trend, in contrast to the warming trend during the early Eocene hyperthermals.

Acknowledgments

This manuscript benefited from comments by Appy Sluijs and two anonymous reviewers on a previous version of this manuscript and comments by the editor on this manuscript. This research used samples and data provided by the ODP. Financial support was provided by the KU Leuven Research Fund to RPS and the DFG to AB (BO2505/8-1, EH 89/20). G. Grützner (BGR) is thanked for preparing samples for LECO analyses.

References

Bornemann, A., Schulte, P., Sprong, J., Steurbaut, E., Youssef, M. and Speijer, R.P., 2009. Latest Danian carbon isotope anomaly and associated environmental change in the southern Tethys (Nile Basin, Egypt). *Journal of the Geological Society*, **166**, 1135-1142.

Caballero, R. and Huber, M., 2013. State-dependent climate sensitivity in past warm climates and its implications for future climate projections. *Proceedings of the National Academy of Sciences*, **110**, 14162-14167.

Chevin, L.-M., Lande, R. and Mace, G.M., 2010. Adaptation, plasticity, and extinction in a changing environment: towards a predictive theory. *PLoS Biology*, **8**, e1000357.

Clyde, W.C., Tong, Y., Snell, K.E., Bowen, G.J., Ting, S., Koch, P.L., Li, Q., Wang, Y. and Meng, J., 2008. An integrated stratigraphic record from the Paleocene of the Chijiang Basin, Jiangxi Province (China): Implications for mammalian turnover and Asian block rotations. *Earth and Planetary Science Letters*, **269**, 554-564.

Corliss, B.H. and Chen, C., 1988. Morphotype patterns of Norwegian Sea deep-sea benthic foraminifera and ecological implications. *Geology*, **16**, 716-719.

D'haenens, S., Bornemann, A., Stassen, P. and Speijer, R.P., 2012. Multiple early Eocene benthic foraminiferal assemblage and $\delta^{13}C$ fluctuations at DSDP Site 401 (Bay of Biscay — NE Atlantic). *Marine Micropaleontology*, **88-89**, 15-35.

D'haenens, S., Bornemann, A., Claeys, P., Röhl, U., Steurbaut, E. and Speijer, R.P., 2014. A transient deep-sea circulation switch during Eocene Thermal Maximum 2. *Paleoceanography*, **29**, 370-388.

DeConto, R.M., Galeotti, S., Pagani, M., Tracy, D., Schaefer, K., Zhang, T., Pollard, D. and Beerling, D.J., 2012. Past extreme warming events linked to massive carbon release from thawing permafrost. *Nature*, **484**, 87-91.

Dickens, G.R., 2003. Rethinking the global carbon cycle with a large, dynamic and microbially mediated gas hydrate capacitor. *Earth and Planetary Science Letters*, **213**, 169-183.

Diefendorf, A.F., Mueller, K.E., Wing, S.L., Koch, P.L. and Freeman, K.H., 2010. Global patterns in leaf ^{13}C discrimination and implications for studies of past and future climate. *Proceedings of the National Academy of Sciences*, **107**, 5738-5743.

Edgar, K.M., Pälike, H. and Wilson, P.A., 2013. Testing the impact of diagenesis on the $\delta^{18}O$ and $\delta^{13}C$ of benthic foraminiferal calcite from a sediment burial depth transect in the equatorial Pacific. *Paleoceanography*, **28**, 468-480.

Erez, J. and Luz, B., 1983. Experimental paleotemperature equation for planktonic foraminifera. *Geochimica et Cosmochimica Acta*, **47**, 1025-1031.

Gibbs, S.J., Bown, P.R., Murphy, B.H., Sluijs, A., Edgar, K.M., Pälike, H., Bolton, C.T. and Zachos, J.C., 2012. Scaled biotic disruption during early Eocene global warming events. *Biogeosciences Discussions*, **9**, 1237-1257.

Hammer, Ø., 2015. PAST reference manual. version 3.08.

Hammer, Ø., Harper, D.A.T., 2006. *Paleontological data analysis.* Blackwell Publishing, Oxford, UK.

Hilgen, F.J., Abels, H.A., Kuiper, K.F., Lourens, L.J. and Wolthers, M., 2015. Towards a stable astronomical time scale for the Paleocene: aligning Shatsky Rise with the Zumaia – Walvis Ridge ODP Site 1262 composite. *Newsletters on Stratigraphy*, **48**, 91-110.

Jehle, S., Bornemann, A., Deprez, A. and Speijer, R.P., 2015. The impact of the Latest Danian Event on planktic foraminiferal faunas at ODP Site 1210 (Shatsky Rise, Pacific Ocean). *PLoS ONE*, **10**, e0141644.

Jennions, S.M., Thomas, E., Schmidt, D.N., Lunt, D. and Ridgwell, A., 2015. Changes in benthic ecosystems and ocean circulation in the Southeast Atlantic across Eocene Thermal Maximum 2. *Paleoceanography*, **30**, 1059-1077.

Lauretano, V., Littler, K., Polling, M., Zachos, J.C. and Lourens, L.J., 2015. Frequency, magnitude and character of hyperthermal events at the onset of the Early Eocene Climatic Optimum. *Climate of the Past*, **11**, 1313-1324.

Littler, K., Röhl, U., Westerhold, T. and Zachos, J.C., 2014. A high-resolution benthic stable-isotope record for the South Atlantic: Implications for orbital-scale changes in Late Paleocene–Early Eocene climate and carbon cycling. *Earth and Planetary Science Letters*, **401**, 18-30.

Lunt, D.J., Valdes, P.J., Jones, T.D., Ridgwell, A., Haywood, A.M., Schmidt, D.N., Marsh, R. and Maslin, M., 2010. CO_2-driven ocean circulation changes as an amplifier of Paleocene-Eocene Thermal Maximum hydrate destabilization. *Geology*, **38**, 875-878.

Lynch, M., Lande, R., 1993. Evolution and extinction in response to environmental change. In: *Biotic interactions and global change* (P. Kareiva, J. Kingsolver and R. Huey, eds.). Sinauer Associates, Sunderland, Massachusetts.

McCarren, H., Thomas, E., Hasegawa, T., Röhl, U. and Zachos, J.C., 2008. Depth dependency of the Paleocene-Eocene carbon isotope excursion: Paired benthic and terrestrial biomarker records (Ocean Drilling Program Leg 208, Walvis Ridge). *Geochemistry, Geophysics, Geosystems*, **9**, Q10008.

McInerney, F.A. and Wing, S.L., 2011. The Paleocene-Eocene Thermal Maximum: a perturbation of carbon cycle, climate, and biosphere with implications for the future. *Annual Review of Earth and Planetary Sciences*, **39**, 489-516.

Monechi, S., Reale, V., Bernaola, G. and Balestra, B., 2013. The Danian/Selandian boundary at Site 1262 (South Atlantic) and in the Tethyan region: biomagnetostratigraphy, evolutionary trends in fasciculiths and environmental effects of the Latest Danian Event. *Marine Micropaleontology*, **98**, 28-40.

Pawlowski, J., Fahrni, J., Lecroq, B., Longet, D., Cornelius, N., Excoffier, L., Cedhagen, T. and Gooday, A.J., 2007. Bipolar gene flow in deep-sea benthic foraminifera. *Molecular Ecology*, **16**, 4089-4096.

Röhl, U., Westerhold, T., Monechi, S., Thomas, E., Zachos, J.C. and Donner, B., 2006. The third early Eocene thermal maximum: Characteristics, timing, and mechanisms of the "X" Event. *Geophysical Research Abstracts*, **8**, 04560.

Schubert, B.A. and Jahren, A.H., 2012. The effect of atmospheric CO_2 concentration on carbon isotope fractionation in C_3 land plants. *Geochimica et Cosmochimica Acta*, **96**, 29-43.

Schulte, P., Schwark, L., Stassen, P., Kouwenhoven, T.J., Bornemann, A. and Speijer, R.P., 2013. Black shale formation during the Latest Danian Event and the Paleocene-Eocene Thermal Maximum in central Egypt: Two of a kind. *Palaeogeography, Palaeoclimatology, Palaeoecology*, **371**, 9-25.

Shackleton, N.J. and Kennett, J.P., 1975. Paleotemperature history of the Cenozoic and the initiation of Antarctic glaciation; oxygen and carbon isotope analyses in DSDP sites 277, 279, and 281. *Initial Reports of the Deep Sea Drilling Project*, **29**, 743-755.

Shackleton, N.J., Hall, M.A., Boersma, A., 1984. Oxygen and carbon isotope data from Leg 74 foraminifers. In: *Initial Reports of the Deep Sea Drilling Project*, **74** (T.C. Moore Jr., P.D. Rabinowitz, et al., eds.) Texas A&M University, Ocean Drilling Program, College Station, Texas.

Shipboard Scientific Party, 2004a. Leg 208 summary. In: *Proceedings of the Ocean Drilling Program, Initial Reports*, **208** (J.C. Zachos, D. Kroon, P. Blum, et al., eds.) Texas A&M University, Ocean Drilling Program, College Station, Texas.

Shipboard Scientific Party, 2004b. Site 1262. In: *Proceedings of the Ocean Drilling Program, Initial Reports*, **208** (J.C. Zachos, D. Kroon, P. Blum, et al., eds.) Texas A&M University, Ocean Drilling Program, College Station, Texas.

Sprong, J., Kouwenhoven, T.J., Bornemann, A., Schulte, P., Stassen, P., Steurbaut, E., Youssef, M. and Speijer, R.P., 2012. Characterization of the Latest Danian Event by means of benthic foraminiferal assemblages along a depth transect at the southern Tethyan margin (Nile Basin, Egypt). *Marine Micropaleontology*, **86-87**, 15-31.

Stap, L., Lourens, L.J., Thomas, E., Sluijs, A., Bohaty, S. and Zachos, J.C., 2010. High-resolution deep-sea carbon and oxygen isotope records of Eocene Thermal Maximum 2 and H2. *Geology*, **38**, 607-610.

Thomas, E., 1998. Biogeography of the late Paleocene benthic foraminiferal extinction. In: *Late Paleocene – early Eocene climatic and biotic events in the marine and terrestrial records* (M.-P. Aubry, S.G. Lucas and W.A. Berggren, eds.). Columbia University Press, New York, New York.

Thomas, E., 2007. Cenozoic mass extinctions in the deep sea: What perturbs the largest habitat on Earth? In: *Large Ecosystem Perturbations: Causes and Consequences* (S. Monechi, R. Coccioni and M. Rampino, eds.). *Geological Society of America Special Paper,* **424**, 1-23.

Voigt, J., Hathorne, E.C., Frank, M. and Holbourn, A., 2016. Minimal influence of recrystallization on middle Miocene benthic foraminiferal stable isotope stratigraphy in the eastern equatorial Pacific. *Paleoceanography*, **31**, 98-114.

von der Heydt, A.S., Köhler, P., van de Wal, R.S.W. and Dijkstra, H.A., 2014. On the state dependency of fast feedback processes in (paleo) climate sensitivity. *Geophysical Research Letters*, **41**, 6484-6492.

Westerhold, T., Röhl, U., Raffi, I., Fornaciari, E., Monechi, S., Reale, V., Bowles, J. and Evans, H.F., 2008. Astronomical calibration of the Paleocene time. *Palaeogeography, Palaeoclimatology, Palaeoecology*, **257**, 377-403.

Westerhold, T., Röhl, U., Donner, B., McCarren, H.K. and Zachos, J.C., 2011. A complete high-resolution Paleocene benthic stable isotope record for the central Pacific (ODP Site 1209). *Paleoceanography*, **26**, PA2216.

Zachos, J.C., McCarren, H., Murphy, B., Röhl, U. and Westerhold, T., 2010. Tempo and scale of late Paleocene and early Eocene carbon isotope cycles: Implications for the origin of hyperthermals. *Earth and Planetary Science Letters*, **299**, 242-249.

Supplementary information (http://dx.doi.org/10.1111/ter.12250)

Appendix S1. Data files: wt% $CaCO_3$, calculation of accumulation rates of planktic and benthic foraminifera, Shannon diversity, NMDS scores, relative abundances of epi- and endobenthic taxa and the most abundant taxa, isotope measurements

Appendix S2. SEM micrographs for uncleaned *Nuttallides truempyi*

Appendix S3. More extensive method treatment